PHYSICAL LAYER SECURITY FOR MULTIHOP UNDERWATER WIRELESS OPTICAL COMMUNICATIONS USING OPTICAL CDMA

Nguyen Van Thang[*], Dang Tien Sy[#], and Pham Thi Thuy Hien[*]
[*]Posts and Telecommunications Institute of Technology
[#]Academy of Military Science and Technology

Abstract— For secure communications, the authors propose a underwater wireless optical communications code-division multiple-access (UOWC/CDMA) system with multiple relay assistance. Relay nodes employ the Chip Detect-and-Forward (CDF) technique to prevent the difficult multiuser decoding procedure. The proposed system performance, in terms of bit-error rate (BER) and transmission confidentiality, is analyzed in our study over fading channel. Therein, oceanic turbulence and beam misalignment between transmitters (Txs) and receivers (Rxs) have a significant negative impact on the reliability of a UWOC network. Additionally, changes in the water refractive index brought on by changes in pressure, water, and temperature can have an impact on the operation of UWOC systems. The performance analysis of a vertical UWOC link subject to Multiple-access interference and background noise is examined in this work. Additionally, we explore optical code-division multiple access (CDMA), which is used to facilitate simultaneous and asynchronous data transmission between sources (such as ships, buoys, unmanned underwater vehicles, divers, and so forth) and the destination. Based on a precise mathematical framework for link modeling that takes into consideration realistic Tx/Rx and channel parameters while accounting for the effects of oceanic turbulence and beam spreading loss conditions, this study was conducted. Moreover, it is shown that choosing the best Tx/Rx parameters is necessary to meet service quality requirements such as BER and transmission confidentiality. The provided findings provide insightful information about the practical considerations of deploying UWOC/ CDMA systems.

Keywords— Underwater optical wireless communications (UOWC), code division multiple access (CDMA), oceanic turbulence.

I. INTRODUCTION

Due to the continued growth of connected human activities, such as environmental monitoring, offshore oil field research, port security, etc., there is an increasing demand for underwater communication networks today. Such networks should make it possible to communicate with submerged cars or get information from submerged sensors. We are concerned with a wide range of data-rate needs within the underwater Internet of Things (IoTs) paradigm with difficult difficulties of unpredictable propagation environment. Underwater optical wireless communication (UOWC), which enables high-speed, low-latency data transfer in such networks, is viewed in this context as an effective complementing technology to acoustic communications over short-to-moderate link ranges [1-3]. In reality, a number of factors, such as water absorption and scattering [4-6], solar background noise [7, 8], maritime turbulence [9], and pointing errors (PEs) [10–12], have an impact on the performance of UOWC links. As a result, effective approaches for reducing these effects are required. This paper focuses on the effects of oceanic turbulence, which dominates the dynamic performance of underwater networks, in addition to analyzing deterministic losses, such as propagation loss and beam spreading loss. We also take into account choosing the right transmitter (Tx) and receiver (Rx) characteristics to reduce the impact of random channel effects.

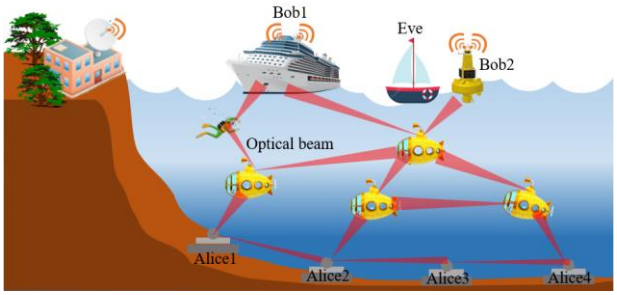

Fig. 1. An example of multirelay-assisted underwater optical wireless communications.

Asynchronous access, scalability, and intrinsic security are some further advantages of OWC/CDMA systems, which have been proposed to allow numerous users to concurrently share the same resource of fading channels [14-17]. The influence of oceanic turbulence has a

Contact author: Nguyen Van Thang
Email: thangnv@ptit.edu.vn
Manuscript received: 6/2023, revised: 7/2023, accepted: 8/2023.

significant negative impact on the performance of OWC/CDMA systems [18]. The rise in bit-error rate (BER) brought on by oceanic turbulence, background noise, and multiple-access interference (MAI), severely reduces the transmission range of OWC/CDMA systems. To solve this issue, a number of methods have been suggested, including forward error correction (FEC), spectral phase encoding, and pulse-position modulation (PPM). PPM has a number of benefits, including non-threshold detection and power efficiency [14-16]. Although PPM-based OWC/CDMA systems must broadcast brief pulses, when transferring high data rates over long distances, the pulse broadening effect has a substantial impact [17]. Better spectral performance and efficiency are also provided by spectral phase-encoded optical CDMA [16]. However, because coherent sources must be used, it is quite challenging. According to the study in [4], FEC can successfully treat physical layer deficits. Due to the large delay and decreased transmission efficiency caused by FEC, its use is currently restricted.

In this study, we suggest using relay-assisted transmission to resolve the OWC/CDMA systems' oceanic turbulence issue. Recently, relay transmission has been proposed in FSO communications as a method to expand the range and dependability of radio frequency lines [19-24]. The performance and range of OWC/CDMA systems can be increased by using relay transmission. When there is no direct line of sight between the users and the receiver, it also helps to implement the system. Bit detect-and-forward (BDF) is frequently used at relay nodes in conventional relay schemes [19-20]. BDF is complicated in relay-assisted OWC/CDMA systems, though, because multiuser detection is needed at each relay node. Therefore, we suggest switching to chip detect and forward (CDF). Relay nodes in relay-assisted OWC/CDMA systems that employ the CDF scheme detect CDMA chips, either "1" or "0," using threshold detection, and then send those chips to the next node in the chain. Additionally, CDF can be effectively combined with the AND detection technique, which is applied at the receiver to lessen the impact of MAI [25].

Additionally, although improved security has frequently been listed as a benefit of OWC and optical CDMA, the standard and extent of security improvements for UOWC/CDMA systems have not been explored. In fact, if a detector is placed within the optical beam's footprint, it is possible to intercept a signal, especially if the optical beam has a broader beam due to the lengthy transmission distance. In this study, we additionally take into account the code interception performance of the suggested UOWC/CDMA systems, which is determined by the likelihood that an eavesdropper will successfully decode the user's whole code word.

In our investigation, we'll look at how relay-assisted UOWC/CDMA systems function in the presence of oceanic turbulence that is modeled as a log-normal fading channel while also accounting for the main physical layer impairments such background noise and MAI. Beam spreading and other effects of the oceanic channel, such as oceanic attenuation, are also taken into account. Analysis will be used to derive the proposed UOWC/CDMA systems' BER and transmission confidentiality expressions. Discussion of numerical findings will take into account a variety of system characteristics, such as transmitted power, relay count, user count, and transmission distance.

II. RELAY-ASSISTED UOWC/CDMA SYSTEM

A. System model

A model of relay-assisted UOWC/CDMA system with k users and N relays is shown in Fig. 2 (right side). Data signal from all k users are transmitted over oceanic channel and collected by the first relay (R_1), where thay are detected and then forwarded to the receiver via other relays (i.e., $R_2, R_3, ..., R_N$). Each user in the UOWC/CDMA system is assigned a unique signature code, which can be either one-dimentional or two-dimensional (2D) one, for encoding its data. With the properties of high cardinality and low peak cross-correlation, 2D wavelength hopping/time spreading (WH/TS) codes have been proposed and adopted in optical CDMA systems [25]. To reduce MAI and ehance security, 2D WH/TS codes are also used in our proposed UOWC/CDMA system, whose block diagram, including a transmitter, a relay, and a receiver, is depicted in Fig. 2 (left side).

At transmitter side, binary data of each user is first modulated with broadband optical signal which is generated from the laser source, at a modulator. Modulated optical signal is then encoded in both wavelength and time domains at a WH/TS encoder, where bit ‘1’ is converted to a chip sequence including chips ‘1’ and ‘0’ while bit ‘0’ is kept unchanged. An optical pulse at a specific wavelength, whose power is P_c , will be transmitted in the case of chip ‘1’ while optical pulse is absent in the case of chip ‘0’.

At the first relay, as depicted in Fig. 2, optical pulses from k users are collected and separated into individual wavelengths at a demultiplexer (λ-DEMUX). The optical signal at each wavelength is then converted to an electrical signal by a photodetector (PD). The electrical signal is then forward a process of CDF by a threshold detector and a laser source. Optical signals from laser sources are combined at a wavelength multiplexer (λ-MUX) before transmitting to the next node. It is worth noting that the transmitted power per chip ‘1’ at the output of R_1 is also kept at the level of P_c . The similar process is performed at other relays (i.e., $R_2, R_3, ..., R_N$) of the system. The CDF process in these relays is not affected by additional MAI as they are only connected to the previous node.

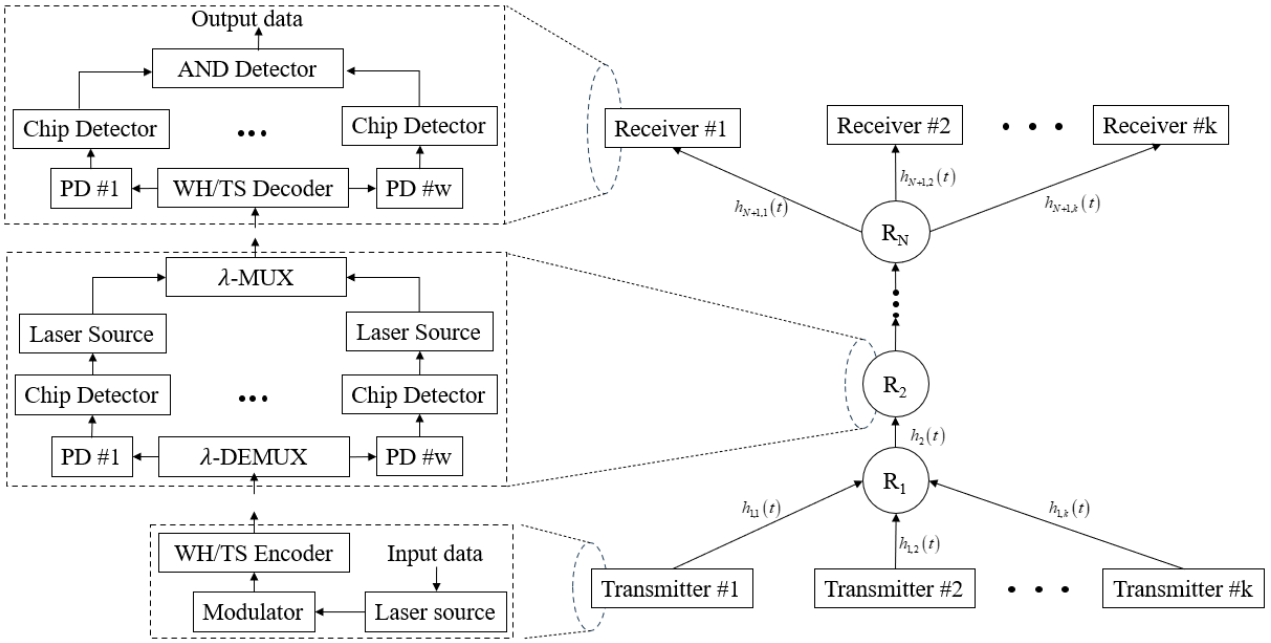

Figure 2. Multihop relay-assisted UOWC CDMA system model and block diagram.

At the receiver side, the binary data from the desired transmitter is decoded at a WH/TS decoder. After passing through the decoder, optical pulse (i.e., chip '1'), whose wavelengths are matched to receiver's signature codes, are collected and separated. In addition, they relative time delays among them are cancelled so that they are aligned in time. Next, these optical pulses are converted to electrical ones at the PDs and then detected at chip detectors. Based on logical levels at the output of the chip detectors, logical AND operation is carried out to detect a bit '1' or a bit '0'

Table 1. WH and TS patterns for $p_s = p_h = 5$

WH pattern	TS pattern
$H_0\lambda_0\lambda_0\lambda_0\lambda_0\lambda_0$	S_0 10000 10000 10000 10000 10000
$H_1\lambda_0\lambda_1\lambda_2\lambda_3\lambda_4$	S_1 10000 01000 00100 00010 00001
$H_2\lambda_0\lambda_2\lambda_4\lambda_1\lambda_3$	S_2 10000 00010 01000 00001 00010
$H_3\lambda_0\lambda_3\lambda_1\lambda_4\lambda_2$	S_3 10000 00010 01000 00001 00100
$H_4\lambda_0\lambda_4\lambda_3\lambda_2\lambda_1$	S_4 10000 00001 00010 00100 01000

B. Prime code

In this paper, we use 2D prime code to provide accessibility for multiple users simultaneously. In detail, each user is assigned a unique code whose length is p_s^2, where p_s is a prime number. A TS pattern can be generated using the linear congruent placement operator to place a pulse within a block as follows

$$c_{xy} = [x, y] \quad x, y = 0,\ 1, ...,\ p_s - 1, \tag{1}$$

where $[\cdot]$ denotes modulo p_s operation, x represents the sequence number within the family of sequences, and y represents the block number for that particular sequence. The algorithm determines the place of a pulse within a block of length p_s. Hence, the prime algorithm produces p_s sequences $(i = 0,1,..., p_s - 1)$ of length p_s^2.

Similarly, a WH pattern is generated from a prime number p_h $(p_s \le p_h)$. In that case, there are p_h wavelengths available for colouring the TS pattern, exactly as there are p_s pulses at one wavelength only and is therefore discareded. Consequently, the number of WH patterns is $p_h - 1$ and a 2D WH/TS code set includes $p_s(p_h - 1)$ distinctive 2D prime codes of length p_s^2. The process of generating the TS and the WH patterns with $p_s = p_h = 5$ is illustrated in Table 1. An example of 2D WH/TS code sequence created by WH pattern H_1 and TS pattern S_2 is $\lambda_0 000\ 000\lambda_1\ 000\lambda_2\ 0\lambda_3 000\ 000\lambda_4 0$.

III. CHANNEL MODELING

This section is an in-depth introduction of underwater UOWC channel model. The channel coefficient, h, is modeled as

$$h = h^l h^{bl} h^t, \tag{2}$$

where h^l and h^{bl} denote propagation loss and beam spreading loss, which are considered as a deterministic value. And, h^t represents the effect of turbulence, which is studied as a random variable.

A. Propagation Loss

Factor h^l represents the attenuation in signal intensity as a result of absorption and scattering. Here, to simplify the derivation of analytical models for the link performance metrics, we approximate h_c by the exponential attenuation model of Beer–Lambert, which neglects the multiple scattering effect [4, 6]

$$h^l = \exp(-Lc_e), \tag{3}$$

where c_e denotes the beam extinction coefficient for a collimated light source, e.g., a laser beam, in contrast to K_d, which is considered for a diffuse light source [26].

B. Oceanic Turbulence

Oceanic turbulence results from random variations of the refractive index along the aquatic medium, which causes fluctuations in the intensity and phase of the average received signal [27]. For a vertical UWOC link, these fluctuations are mostly due to the variations in water temperature and salinity with depth. Based on the profiles of temperature and salinity in the Argo database [28] for different geographical locations and over a long period of time, the log-normal PDF shows a good match with the majority of measured temperature and salinity gradients [29]. We, hence, model h_t by a log-normal distribution, that is,

$$h_t = \exp(T), \tag{4}$$

where T denotes the log-amplitude coefficient of turbulence, following the Gaussian distribution $N(\mu_T, \sigma_T^2)$. The PDF of h_t is

$$f_{h_t}(h_t) = \frac{1}{h_t\sqrt{2\pi\sigma_T^2}}\exp\left(-\frac{\left(\ln(h_t)-\mu_T\right)^2}{2\sigma_T^2}\right). \tag{5}$$

Note that other models have been proposed for the cases of moderate-to-strong turbulence, e.g., the gamma-gamma PDF in [30].

Following the approach in [30], and as illustrated in Fig. 2, the channel is considered a cascade of layers with different mean and variance turbulence parameters, which are assumed to be unchanged within each layer. Assume a total of K layers, with the k-th layer of thickness L_k (where $L = \sum_{u=1}^{U} L_u$), mean μ_{T_u}, and variance $\sigma_{T_u}^2$. The PDF of the corresponding channel coefficient h_{T_u} is

$$f_{h_{t_u}}(h_{t_u}) = \frac{1}{h_{t_u}\sqrt{2\pi\sigma_{T_u}^2}}\exp\left(-\frac{\left(\ln(h_{t_u})-\mu_{T_u}\right)^2}{2\sigma_{T_u}^2}\right). \tag{6}$$

The relationship between $\sigma_{T_u}^2$ and the scintillation index of the k-th layer $\sigma_{I_u}^2$ is given by [31]

$$\sigma_{T_u}^2 = 0.25\ln\left(1+\sigma_{I_u}^2\right) \approx 0.25\sigma_{I_u}^2 \quad \text{for } \sigma_{I_u}^2 \square\ 1.$$

Note that this relationship is valid for the weak turbulence regime, i.e., for $\sigma_{I_u}^2 < 1$. Assuming independent, non-identically distributed h_{T_u}, μ_T, and σ_T^2 in Eq. (5) are [30]

$$\begin{cases} \mu_T = \sum_{u=1}^{U} 2\mu_{T_u} \\ \sigma_T^2 = \sum_{u=1}^{U} 4\sigma_{T_u}^2 \end{cases} \tag{7}$$

To normalize the fading coefficient, i.e., to have $E\{h_{T_u}\} = 1$, we set $\mu_{T_u} = -\sigma_{T_u}^2$.

A well-known method to reduce the scintillation effect on the received signal is aperture averaging, by using an Rx aperture diameter D_r larger than the correlation width of the irradiance fluctuations ρ_c [32]. For a horizontal link and under weak turbulence conditions, the correlation width for a Gaussian beam is given by $\rho_c \sim \sqrt{L/K_w}$, where K_w is the wave number. A few previous works have studied the effect of aperture averaging for horizontal UWOC links [33-36]. To investigate the efficiency of aperture averaging in reducing the oceanic turbulence effect in the considered application scenario, we assume that the Rx uses a Gaussian lens, which is a combination of a thin lens with a Gaussian limiting aperture (i.e., a soft aperture) [36].

Assuming a large enough photodetector (PD) active area [37], to obtain the PDF of Eq. (5) while accounting for aperture averaging, first the scintillation indices $\sigma_{T_u}^2(D_r)$ corresponding to each of the u-th layer should be calculated in Eq. (B1) in Appendix B [13].

C. Beam Spreading and Pointing Error Loss

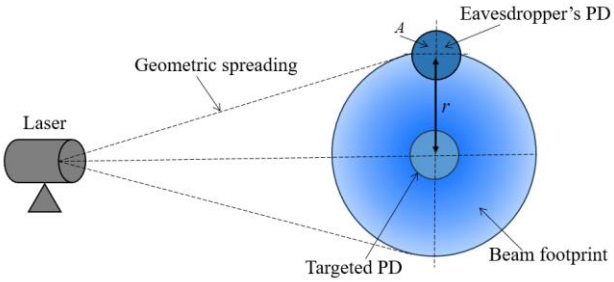

Figure 3. Position of PDs and beam footprint on the detector plane at the distance of L_{owc}.

To compute the fraction of collected power by a desired user and an eavesdropper, we consider a circular detection aperture of radius a and a Gaussian beam profile at the receiver as shown in Fig. 3. For the Gaussian beam, the nomalized spatial distribution of the transmiited intensity at the distance L_{owc} from the transmitter is given by

$$I_{beam}(\rho; D) = \frac{2}{\pi\omega_D^2}\exp\left(-\frac{2\|\rho\|}{\omega_D^2}\right), \tag{8}$$

where ω_L is the beam size at the distance L_{owc}. ρ is the radial vector from the center of beam footprint and $\|.\|$ defines the expression of Euclidean norm. The beam spreading loss is quantified by the fraction of power collected by the detector $h_{bl}(.)$. It not only depends on the beam size but also the relative position between the centers of the detector and the beam footprint, which is known as pointing error. Denoting r as the pointing error, $h_{bl}(.)$ can be determined as

$$h_{bl}(r; D) = \int_A I_{beam}(\rho - r; D)\, d\rho, \tag{9}$$

where A is the area of detector. The Gaussian form of $h_{bl}(.)$ is written as

$$h_{bl}(r; D) \approx A_0 \exp\left(-\frac{2r^2}{\omega_{Leq}^2}\right), \tag{10}$$

where $\omega_{Leq}^2 = \omega_D^2(\sqrt{\pi}erf(v))/2v\exp(-v^2)$ defines the equivalent beam width at the destination. $A_0 = [erf(v)]^2$ and $v = \sqrt{\pi}a/\sqrt{2}\omega_D$ in which a is the radius of the detection aperture at the GS, r is the distance between the center of the beam footprint and the detector. A_0 denotes the fraction of collected power at $r = 0$.

IV. SYSTEM PERFORMANCE ANALYSIS

A. Bit error rate

In this subsection, the proposed system BER is analytically derived. Among k users, one user is assumed

to be the desired user while $k-1$ remaining ones are probable interfering users. The total BER is conditioned on the events: k users among the $(k-1)$ probable interfering users may transmit a data bit '1', which follows a binomial distribution. Under the assumption that theprobabilities of transmitting bit '1' and bit '0' are equally likely for all users, the BER at the receiver can be calculated as

$$\mathrm{BER}=\sum_{i=1}^{k-1}\left\{\binom{k-1}{i}2^{1-k}\frac{1}{2}\left[p_{pe}\left(0|1,k\right)+p_{be}\left(1|0,k\right)\right]\right\}, \quad (11)$$

where $p_{pe}\left(0|1,k\right)$ and $p_{pe}\left(1|0,k\right)$ are the conditional bit error probabilities when detecting bit '1' and bit '0' at the receiver, respectively. In the case of AND detection shown in Fig. 2, logical AND operation is carried out on all '1' chip positions of the desired code to detect a bit '1' [25]. Conditional bit error probabilities therefore can be expressed in terms of the conditional chip error probabilities (CEPs) and for AND detection as

$$p_{pe}\left(0|1,k\right)=\sum_{j=1}^{p_s}\binom{p_s}{j}\left[p_{e2e}\left(0|1,k\right)\right]^{j}\left[1-p_{e2e}\left(0|1,k\right)\right]^{p_s-j},$$

$$p_{pe}\left(1|0,k\right)=\prod_{j=1}^{p_s}p_{e2e}\left(0|1,k\right), \quad (12)$$

where $p_{e2e}\left(0|1,k\right)$ and $p_{e2e}\left(1|0,k\right)$ are end-to-end CEPs when the desired user transmits chip '1' but detects chip '0' and transmits chip '0' but detects chip '1'. It is clear that these probabilities depend on the CEPs of all hops from the desired transmitter to the receiver.

B. CEP for the first hop

CEP for the first hop is determined at the first relay (R_1). At the first hop, CEP is affected by not only background noise but also MAI from interfering users. We assume that the transmitted power per pulse (P_c) and the distance to R_1 are identical for both the desired user and $(k-1)$ remaining users. In addition, among the k users transmitting bit '1', n interfering users may have a pulse overlapping the chip of interest, where $n=\mathrm{binom}\left(k,p_{\mathrm{cov}}\right)$ and p_{cov} is the probability that desired user's chip is overlapped by an interfering user's chip. For the case of 2D WH/TS prime code, $p_{\mathrm{cov}}=\mu_\lambda/p_s^3$ [25], where μ_λ is the average number of wavelengths common to a pair of two codes and, under the condition that $p_h>p_s$, can be estimated as [25]

$$\mu_\lambda=\frac{1}{\binom{p_h}{p_s}}\left\{\begin{array}{l}\binom{p_h-1}{p_s-1}\dfrac{\left(p_h-1\right)\left(p_s-2\right)+\left(p_h+2\right)}{p_h-2}\\ +\binom{p_h-1}{p_s}\dfrac{p_s\left(p_h-1\right)}{p_h-2}\end{array}\right\}. \quad (13)$$

In the special case that $p_h=p_s$, μ_λ equal to p_s , therefore $p_{\mathrm{cov}}=1/p_s^2$.

Given k users transmitting bit '1', n can vary from 1 to k , therefore CEPs for the first hop can be computed as

$$p_{ce-1}\left(1|0,k\right)=\sum_{n=1}^{k}\left\{\binom{k}{n}p_{\mathrm{cov}}^{n}\left(1-p_{\mathrm{cov}}\right)^{k-n}p_{ce}\left(1|0,n\right)\right\}, \quad (14)$$

$$p_{ce-1}\left(0|1,k\right)=\sum_{n=1}^{k}\left\{\binom{k}{n}p_{\mathrm{cov}}^{n}\left(1-p_{\mathrm{cov}}\right)^{k-n}p_{ce}\left(0|1,n\right)\right\}, \quad (15)$$

where $p_{ce-1}\left(1|0,k\right)$ and $p_{ce-1}\left(0|1,k\right)$ are the conditional CEPs when dectecting chip '1' and chip '0', respectively.

The conditional CEPs are governed by the received power per chip at the input of the relay R_1 , which can be expressed as

$$P_{1(0)}=\sum_{i=1}^{n}h_{1,i}P_c+P_b=h_{1(0)}P_c+P_b, \quad (16)$$

$$P_{1(1)}=h_{1,d}P_c+\sum_{i=1}^{n}h_{1,i}P_c+P_b=h_{1(1)}P_c+P_b, \quad (17)$$

where $P_{1(0)}$ and $P_{1(1)}$ are the received optical powers when desired user transmits chip '0' and chip '1', espectively. P_b is the average background power. $h_{1,i}$ denotes the oceanic channel coefficient of the *i*-th interfering user and we assume that it has the same pdf with the desired one's (i.e. $h_{1,d}$). Here, the sums of n or $(n+1)$ log-normal random variables can be approximated into a single log-normal random variable denoted as $h_{1(0)}$ or $h_{1(1)}$ (the detail about this approximation is given by (34) in Appendix).

When received optical singals pass through the PD, they are converted to the electrical currents which can be expressed as

$$I_{1(0)}=\Re h_{1(0)}P_c, \quad (18)$$

$$I_{1(1)}=\Re h_{1(1)}P_c, \quad (19)$$

where $I_{1(0)}$ and $I_{1(1)}$ are electrical signals respectively converted from $P_{1(0)}$ and $P_{1(1)}$ thanks to the PD. Besides, background power causes the background noise, whose variance can be written as

$$p_{ce}\left(1|0,n\right)=\int_0^\infty\int_{I_D}^\infty f_P\left(h_{1(0)}^a\right)\frac{1}{\sqrt{2\pi\sigma_b^2}}\times\exp\left(-\frac{\left(x-I_{1(0)}\right)^2}{2\sigma_b^2}\right)dh_{1(0)}^a dx, \quad (20)$$

$$p_{ce}\left(0|1,n\right)=\int_0^\infty\int_{-\infty}^{I_D} f_P\left(h_{1(1)}^a\right)\frac{1}{\sqrt{2\pi\sigma_b^2}}\times\exp\left(-\frac{\left(x-I_{1(1)}\right)^2}{2\sigma_b^2}\right)dh_{1(1)}^a dx, \quad (21)$$

where I_D is the chip detection threshold, which is assumed to be fixed. $f_P\left(h_{1(0)}^a\right)$, $f_P\left(h_{1(1)}^a\right)$ correspond to the joint pdf of log-normal vector of length n and $n+1$, respectively. It is worth noting that $h_{1(0)}=h_1^l h_1^p h_{1(0)}^a$ and $h_{1(1)}=h_1^l h_1^p h_{1(1)}^a$, where h_1^l and h_1^p are the channel loss coefficient and the fraction of the collected power of the first hop, respectively.

Performing $z_0 = \ln\left(h^a_{1(0)}\right)$ and $z_1 = \ln\left(h^a_{1(1)}\right)$ transformations, we have

$$p_{ce}\left(1|0,n\right) = \int_{-\infty}^{\infty} \Omega\left(z_0, \mu_{z_0}, \sigma^2_{z_0}\right) \times Q\left(\frac{I_D - \Re P_c h_1^l h_1^p \exp\left(z_0\right)}{\sigma_b}\right) dz_0, \quad (22)$$

$$p_{ce}\left(0|1,n\right) = \int_{-\infty}^{\infty} \Omega\left(z_1, \mu_{z_1}, \sigma^2_{z_1}\right) \times Q\left(\frac{I_D - \Re P_c h_1^l h_1^p \exp\left(z_1\right)}{\sigma_b}\right) dz_1, \quad (23)$$

Where $Q(u) = \int_u^{\infty} \Omega(x,0,1)dx$. Furthermore, (22) and (23) can be approximated by Gauss-Hermit quadrature formula (shown in Appendix)

$$p_{ce}\left(1|0,n\right) \approx \sum_{t=1}^{v} \frac{g_t}{\sqrt{\pi}} Q\left(\frac{I_D - \Re P_c h_1^l h_1^p \exp\left(\mu_{z_0} + m_t \sigma_{z_0}\sqrt{2}\right)}{\sigma_b}\right), \quad (24)$$

$$p_{ce}\left(0|1,n\right) \approx \sum_{t=1}^{v} \frac{g_t}{\sqrt{\pi}} Q\left(\frac{\Re P_c h_1^l h_1^p \exp\left(\mu_{z_1} + m_t \sigma_{z_1}\sqrt{2}\right) - I_D}{\sigma_b}\right), \quad (25)$$

Where m_t and g_t are the zero of the *t*-th order Hermite polynomial value and the weight factor for the *t*-th order approximation, respectively.

a) CEP for the m-th hop (m = 2, 3, …., N+1)

For the *m*-hop with m = 2, 3, …., *N+1*, there is no additional MAI but still having the presence of oceanic channel effects and background noise. Therefore, the received current at relay (R_i) can be expressed as

$$I_m = \begin{bmatrix} I_{m(0)} \\ I_{m(1)} \end{bmatrix} = \begin{bmatrix} n_b \\ \Re P_c h_m + n_b \end{bmatrix} \quad (26)$$

By following the mathematical transformations as presented in the previous subsection, we can derive the CEP for the *m*-th hop as

$$p_{ce-m}\left(1|0,k\right) = Q\left(\frac{I_D}{\sigma_b}\right), \quad (27)$$

$$p_{ce-m}\left(0|1,k\right) \approx \sum_{t=1}^{v} \frac{g_t}{\sqrt{\pi}} Q\left(\frac{\Re P_c h_i^l \exp\left(\mu_z + m_t \sigma_z \sqrt{2}\right) - I_D}{\sigma_b}\right). \quad (28)$$

b) End-to-end CEP

In Multi-relay-assisted UOWC/CDMA systems, there is a possibility that the receiver may still detect correctly a chip although that chip is detected incorrectly in an even number of times in the previous relays. For the worst-case performance, we consider that the end-to-end CEP is the probability that chips are transmitted without error between any pair of two consecutive relays, and it can be expressed as

$$P_{e2e}\left(1|0,k\right) = 1 - \prod_{m=1}^{N+1}\left(1 - p_{ce-m}\left(1|0,k\right)\right), \quad (29)$$

$$P_{e2e}\left(0|1,k\right) = 1 - \prod_{m=1}^{N+1}\left(1 - p_{ce-m}\left(0|1,k\right)\right), \quad (30)$$

Table 2. System parameters

Name	Symbol	Value
Bolzmann's constant	K	1.38×10^{-23} $WHz^{-1}K^{-1}$
Electronic charge	q	$1.6x10^{-19}$ C
Light velocity	c	$3x10^8$ m/s
Load resistance	R_L	50 Ohm
Temperature	T	300 K
PD responsivity	R	0.6 A/W
Optical wavelength	λ	450 nm
Transmission distance	L_{owc}	30 m
Aperture radius	a	10 cm
Background power	P_b	-30 dBm

V. SECURITY ANALYSIS

Security is a quantitative issue, and there is yet no exact, acceptable quantification of QKD security under all probable assaults. Because the system under consideration is based on ordinary FSO systems with classical signals, simple physical-layer eavesdropping is the most effective technique. Several essential assaults in FSO communications, such as collective and coherent attacks, cannot be carried out using the classical signal eavesdropping method [39]. Furthermore, there are two types of unauthorized receiver assault when using dual-threshold/direct detection (DT/DD) receivers: (1) beam-splitting attack and (2) intercept-resend attack. The beam-splitting attack is taken into account in our study.

To demodulate user's data, an eavesdropper has to detect exactly the code word of the user. By locating a receiver in the coverage of the optical beam, the eavesdropper is able to detect the coded transmissions of users to perform the necessary calculations and derive the code from this information. The resulting code will have some probability of error, which depends strongly on the signal-to-noise ratio at the eavesdropper's receiver.

Similar to [25], in our analysis, we consider the worst-case assumption from a security perspective (i.e., the best possible performance for the eavesdropper) that the eavesdropper is able to synchronise the user's signal, locate the beginning and ending of a data bit, and then can sample the detector output precisely at the end of each code chip time. Code interception performance is calculated based on the average probability that the eavesdropper can detect the user's entire code word with no errors, denoted by Pcorrect. This probability, therefore, can be computed from the probability of missing a transmitted pulse in a given chip time (PM) and the probability of falsely detecting a pulse in a chip time where none was transmitted (PF) as

$$P_{correct} = \sum_{i=1}^{k} \binom{k-1}{i} 2^{1-k} \left(1-P_M\right)^{p_s} \left(1-P_F\right)^{p_s^2 p_h - p_s}, \quad (31)$$

where the first term represents the probability of not missing any of the pulses that are transmitted during a data bit; the second term is the probability of not falsely detecting pulses in any of the $p_s^2 p_h - p_s$ chip time where pulses are not transmitted during a data bit.

Assuming that the eavesdropper places its receiver next to the node m (a relay or destination) to detect the coded transmissions. The distance between the eavesdropper's receiver and that of relays (or destination) is denoted as r (see Fig. 3), thus the fraction of power collected by the eavesdropper is $h_p(r;z)$ where r is larger than zero. P_M and P_F, are the accumulated CEPs that the user transmits chip '1' but the eavesdropper detects chip '0' and the user transmits chip '0' but the eavesdropper detects chip '1', respectively. P_M and P_F, therefore, can be expressed as

$$P_{M-m} = 1 - \prod_{j=1}^{m} \left(1 - p_{ce-j}\left(1|0,k\right)\right), \quad (32)$$

$$P_{F-m} = 1 - \prod_{j=1}^{m} \left(1 - p_{ce-j}\left(0|1,k\right)\right). \quad (33)$$

VI. RESULTS AND DISCUSSION

This section presents numerical results of the proposed system BER and security analysis. We assume the distance of L_{owc} m from the source to the destination and the consecutive nodes are equidistant along the path. The numerical results are considered under a constraint on the fixed energy per bit E_b. Because there are p_s pulses in one bit duration, which are assumed to have equal power, the relation between the energy per bit and the power per chip is given by $P_c = \left(E_b / p_s\right)/T_c$, where $\left(E_b / p_s\right)$ and T_c are the chip energy and chip duration, respectively. In addition, the threshold detection level I_D can be calculated as $I_D = \Re P_c h^l D$, where D is the normalized threshold and set at the same level for all hops along the transmission path. The effective electrical bandwidth, B_e, is fixed at 70% of the chip rate [25]. The relation between the chip rate R_c and the bit rate per user (R_b) can be expressed as $R_c = R_b p_s^2$, where (p_s^2) is the code length. Other system parameters and constants used in the analysis are shown in Table 2.

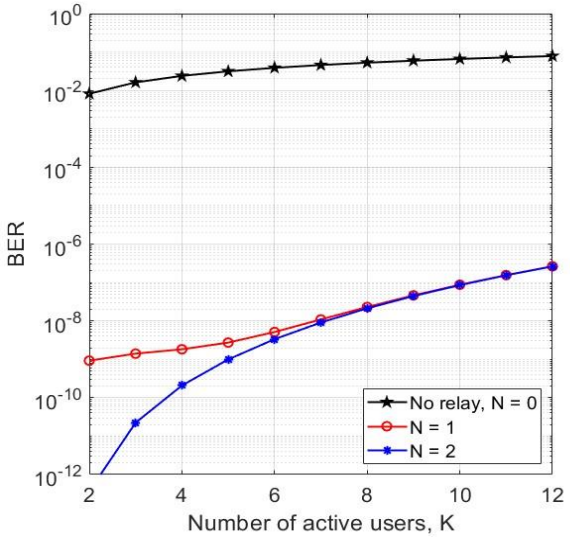

Figure 4. BER versus the number of active users (k) with $E_b = -130\,dBJ$, $R_b = 5\,Gbps$, $p_s = 7$, and $p_h = 7$.

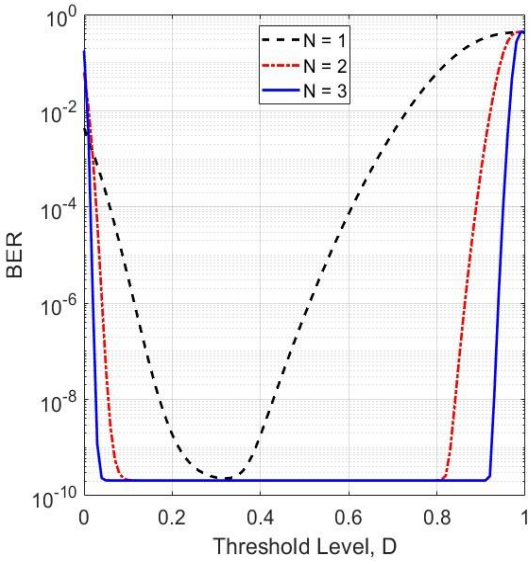

Figure 5. The relationship between BER and nomalized threshold (D) with $E_b = -130\,dBJ$, $k = 4$, $R_b = 5\,Gbps$, $p_s = 7$, and $p_h = 7$.

First, the benefits of using relay transmission are quantified in Fig. 4, which also shows BER versus the number of active users k. Under the impacts of physical layer impairments, including oceanic turbulence, MAI, and background noise, BER of UOWC/CDMA systems without relaying is very high even when the number of users is small. On the other hand, the use of relay transmission can help to reduce BER significantly. As a result, the relay-assisted UOWC/CDMA systems with one or two relays can support more than more than 10 users with BER of 10^{-6} when L_{owc} = 30 m and R_b = 5 Gbps.

Fig. 5 investigates the system BER against the normalized threshold with the number of relays varying from 1 to 3. To achieve low BER, the normalized threshold should be chosen properly. If D is too small, system's performance is degraded due to detecting chip '1' when none was transmitted. In the case when D is too large, error detection is induced by falsely detecting chip '0' when chip '1' was transmitted. The optimum threshold selection depends on parameter settings, especially the number of relays. When the number of relays is large enough, BER reaches the floor, and the selection of threshold can be chosen from a wide range of values.

To further examine the gain of using relay transmission in terms of transmission distance, Fig. 6 demonstrates the BER as a function of L_{owc} with $E_b = -130$ dBJ. In this case, BER floor is governed by the number of active users that is related to the strength of MAI. It is seen that the transmission distance that UOWC/CDMA systems can support (at a specific BER) increases with the number of relays. For example, at k = 4 users and BER of 10^{-6}, the transmission distance increases from 3.5 to 5.2 km when the number of relays increases from 1 to 2. Obviously, longer transmission distance can be achieved by deploying more relays.

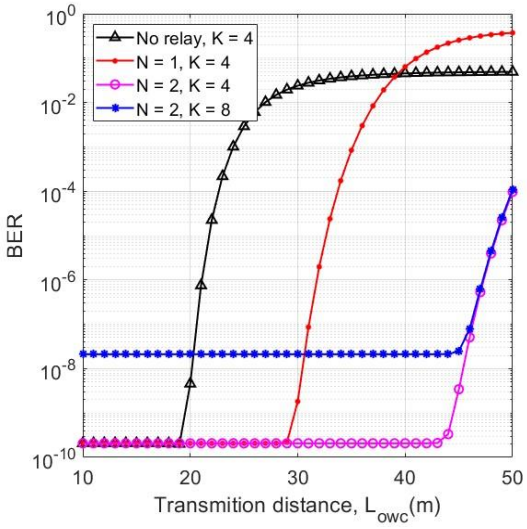

Figure 6. The impact of transmission distance on BER with $E_b = -130\,dBJ$, $R_b = 5\,Gbps$, $p_s = 7$, *and* $p_h = 7$.

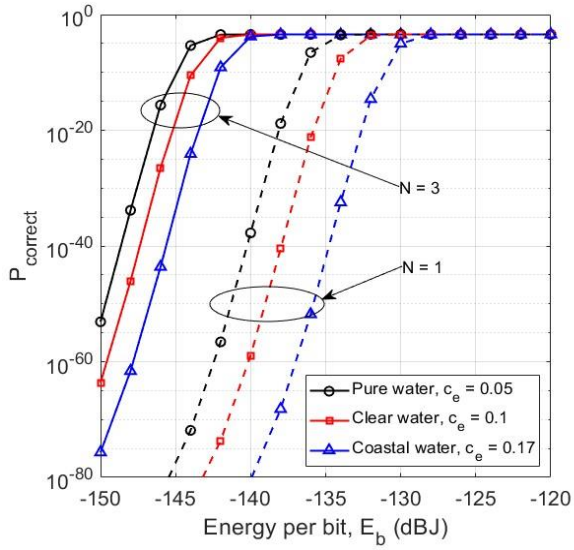

Figure 7. $P_{correct}$ *versus total transmitted power per bit with* $E_b = -130\,dBJ$, $k = 4$, $R_b = 5\,Gbps$, $p_s = 7$, *and* $p_h = 7$.

Fig. 7 depicts the average probability that the eavesdropper can detect the user's entire code word with no errors $P_{correct}$ against the transmitted power per bit P_s. Several underwater environment conditions are investigated in this result to show how the impact of propagation loss on the security performance. Obviously, the pure water allows highest security due to the loss is smallest. Confidentiality is also decreased when the eavesdropper's receiver is located near the targeted receiver. This is because the fraction of optical power that reaches unauthorised receiver increases with c_e as shown in (3).

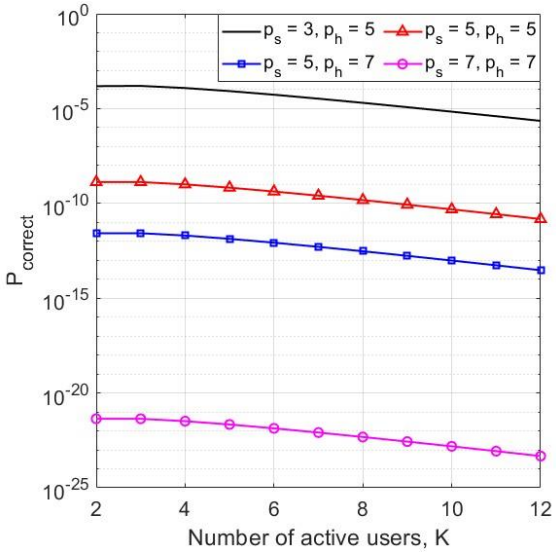

Figure 8. The relationship between $P_{correct}$ *and number of active users (k) with* $E_b = -140\,dBJ$, $R_b = 5\,Gbps$, $p_s = 7$, *and* $p_h = 7$.

Finally, we investigate $P_{correct}$ as a function of the number of active users k with different code sets, that is, different value of p_s and p_h as shown in Fig. 8. Thanks to the effect of MAI from interfering users, $P_{correct}$ is reduced when k increases. In addition, BER is reduced by increasing either ps or ph. When p_s is increased, $P_{correct}$ is reduced more significantly. Moreover, the number of supportable users at a specific value of $P_{correct}$ can be determined from this result. As shown in the figure, the system using p_s = 7 and p_h = 7 (i.e., 7 wavelengths) can support 12 users with the $P_{correct}$ of 10^{-20}, which is under twice times the required number of wavelengths. This is an advantage of UOWC systems using CDMA compared with the ones using wavelength-division multiple-access.

VII. CONCLUDING REMARK

We considered a vertical UWOC link subject to propagation loss, beam spreading and pointing loss, oceanic turbulence-induced fading, MAI, and receiver noise investigated the BER performance of the link under different realistic operational conditions. Analytical expressions were derived for the link probability of bit error. Also, we elucidated the impact of oceanic turbulence, where, in particular, it was shown that the turbulence effect is practically negligible when using a lens at the Rx, even of a relatively small size, due to the aperture averaging effect. The interest in optimum parameter selection for the Tx/Rx was further investigated, allowing significant performance improvement by making a compromise, especially regarding the effects of adverse issues. Furthermore, we investigated CDMA in UOWC system which is improved by reducing the effect of MAI.

Based on an accurate mathematical expression for optical channel modeling that taking into account channel parameters under the effects of the propagation loss, oceanic turbulence-induced fading and beam spreading loss conditions. Furthermore, we provide an analytical expression for computing the bit error rate (BER). The numerical results give valuable insight into the practical aspects of the implementation of UWOC networks using CDMA for the future six-generation (6G) network.

The extension of this study to the case of downlink transmission, i.e., from the AUV to the buoy, is the subject of future research, which is, nevertheless, less problematic. As a matter of fact, our choice of focusing on the uplink is justified by the fact that the surface platform is much more subject to inclinations and displacements compared to the underwater platform; therefore, the link performance is more considerably subject to beam spreading loss. It could be interesting to apply more mitigation techniques such as relay transmission scheme, diversity, hybrid acoustic/OWC system, etc., to enhance the system performance.

REFERENCES

[1] M. A. Khalighi, C. J. Gabriel, L. M. Pessoa, and B. Silva, "Underwater visible light communications, channel modeling and system design," in Visible Light Communications: Theory and Applications (CRC Press, 2017), pp. 337–372

[2] M. A. Khalighi, C. Gabriel, T. Hamza, S. Bourennane, P. Léon, and V. Rigaud, "Underwater wireless optical communication; recent advances and remaining challenges (Invited paper)," in IEEE International Conference on Transparent Optical Networks (ICTON), Graz, Austria, 2014.

[3] X. Sun, C. H. Kang, M. Kong, O. Alkhazragi, Y. Guo, M. Ouhssain, Y. Weng, B. H. Jones, T. K. Ng, and B. S. Ooi, "A review on practical considerations and solutions in underwater wireless optical commu- nication," J. Lightwave Technol. 38, 421–431 (2020).

[4] B. Cochenour, L. Mullen, and J. Muth, "Temporal response of the underwater optical channel for high-bandwidth wireless laser communications," IEEE J. Ocean. Eng. 38, 730–742 (2013).

[5] M. Doniec, M. Angermann, and D. Rus, "An end-to-end signal strength model for underwater optical communications," IEEE J. Ocean. Eng. 38, 743–757 (2013).

[6] C. Gabriel, M. A. Khalighi, S. Bourennane, P. Léon, and V. Rigaud, "Monte-Carlo-based channel characterization for underwater optical communication systems," J. Opt. Commun. Netw. 5, 1–12 (2013).

[7] T. Hamza, M. A. Khalighi, S. Bourennane, P. Léon, and J. Opderbecke, "Investigation of solar noise impact on the perform- ance of underwater wireless optical communication links," Opt. Express 24, 25832–25845 (2016).

[8] J. W. Giles and I. N. Bankman, "Underwater optical communi- cation systems. Part 2: basic design considerations," in Military Communications Conference (MILCOM), Atlantic City, New Jersey, 2005, pp. 1700–1705.

[9] O. Korotkova, N. Farwell, and E. Shchepakina, "Light scintillation in oceanic turbulence," Waves Random Complex Media 22, 260–266 (2012).

[10] C. Gabriel, M. A. Khalighi, S. Bourennane, P. Léon, and V. Rigaud, "Misalignment considerations on point-to-point underwater wireless optical links," in IEEE OCEANS Conference, Bergen, Norway, 2013.

[11] S. Tang, Y. Dong, and X. Zhang, "On link misalignment for under- water wireless optical communications," IEEE Commun. Lett. 16, 1688–1690 (2012).

[12] A. S. Ghazy, S. Hranilovic, and M. A. Khalighi, "Angular MIMO for underwater wireless optical communications: link modelling and tracking," IEEE J. Ocean. Eng. 46, 1391–1407 (2021).

[13] I. C. Ijeh, M. A. Khalighi, M. Elamassie, S. Hranilovic, and M. Uysal, "Outage probability analysis of a vertical underwater wireless optical link subject to oceanic turbulence and pointing errors," IEEE/OSA J. Opt. Commun. Netw., vol. 14, no. 6, pp. 439 – 453, June, 2022.

[14] Ohtsuki, T.: 'Performance analysis of atmospheric optical PPM CDMA systems', J. Lightwave Technol., 2005, 21, (2), pp. 406–411

[15] Ohba, K., Hirano, T., Miyazawa, T., Sasase, I.: 'A symbol detection scheme to mitigate effects of scintillations and MAIs in optical atmospheric PPM-CDMA systems.' Proc. IEEE Globecom, St. Louis, MO, November/December 2005, pp. 1999–2003

[16] Pham, A.T., Luu, T.A., Dang, N.T.: 'Performance bound for turbo-coded 2-D FSO/CDMA systems over atmospheric turbulence channel', IEICE Trans. Fundam., 2010, 93-A, (12), pp. 2696–2699

[17] Dang, N.T., Pham, A.T.: 'Performance improvement of FSO/CDMA systems over dispersive turbulence channel using multi-wavelength PPM signaling', OSA Opt. Exp., 2012, 20, (24), pp. 26786–26797

[18] N. V. Thang and P. T. T. Hien, "Performance of underwater wireless optical IoT networks using CDMA," Journal of Science and Technology on Information and Communications, no. 2, pp. 24–30, 2022.

[19] Akella, J., Yuksel, M., Kalyanaraman, S.: 'Error analysis of multi-hop free-space optical communication'. Proc. of IEEE Int. Conf. on Communication, 2005, pp. 1777–1781

[20] Safari, M., Uysal, M.: 'Relay-assisted free-space optical communication', IEEE Trans. Wirel. Commun., 2008, 7, (12), pp. 5441–5449

[21] Datsikas, C.K., Peppas, K.P., Sagias, N.C., Tombras, G.S.: 'Serial free-space optical relaying communications over Gamma-Gamma atmospheric turbulence channels', J. Opt. Commun. Netw., 2010, 2, (8), pp. 576–586

[22] Feng, M., Wang, J.B., Sheng, M., Cao, L.L., Xie, X.X., Chen, M.: 'Outageperformance for parallel relay-assisted free-space optical communications in strong turbulence with pointing errors'. Proc. of International Conf. on Wireless Commun. and Signal Processing (WCSP), 2011, pp. 1–5

[23] Chatzidiamantis, N.D., Michalopoulos, D.S., Kriezis, E.E., Karagiannidis, G.K., Schober, R.: 'Relay selection protocols for relay-assisted free-space optical systems', IEEE/OSA J. Opt Commun. Netw., 2013, 5, (1), pp. 92–103 15 Kashani, M., Safari, M., Uysal, M.: 'Optimal relay placement in cooperative free-space optical communication systems', IEEE J. Opt. Commun. Netw., 2013, 5, (1), pp. 37–47

[24] Meenakshi, M., Andonovic, I.: 'Effect of physical layer impairments on SUM and AND detection strategies for 2-D optical CDMA', IEEE Photon. Technol. Lett., 2005, 17, (5), pp. 1112–1114.

[25] Hien T. T. Pham, Phuc V. Trinh, Ngoc T. Dang, and Anh T. Pham, "Secured Relay-Assisted Atmospheric Optical CDMA Systems over Turbulence Channels", IET Optoelectronics, Special Issue on Optical Wireless Communications, Vol. 9, Iss. 5, pp. 241-248, Oct. 2015.

[26] C. Mobley, E. Boss, and C. Roesler, "Ocean optics web book" [Accessed 16 December 2021], http://www.oceanopticsbook.info/.

[27] H. Kaushal and G. Kaddoum, "Underwater optical wireless communication," IEEE Access 4, 1518–1547 (2016).

[28] "Global ocean data assimilation experiment (GODAE)" [Accessed 15 April 2022], https://nrlgodae1.nrlmry.navy.mil/index.html
[29] M. V. Jamali, A. Mirani, A. Parsay, B. Abolhassani, P. Nabavi, A. Chisari, P. Khorramshahi, S. Abdollahramezani, and J. A. Salehi, "Statistical studies of fading in underwater wireless optical channels in the presence of air bubble, temperature and salinity random variations," IEEE Trans. Commun. 66, 4706–4723 (2018).
[30] M. Elamassie and M. Uysal, "Vertical underwater visible light communication links: channel modeling and performance analysis," IEEE Trans. Commun. 19, 6948–6959 (2020).
[31] L. C. Andrews, R. L. Phillips, and C. Y. Hopen, Laser Beam Scintillation with Applications (SPIE, 2001).
[32] M.-A. Khalighi, N. Schwartz, N. Aitamer, and S. Bourennane, "Fading reduction by aperture averaging and spatial diversity in optical wireless systems," J. Opt. Commun. Netw. 1, 580–593, (2009).
[33] M. C. Gökçe and Y. Baykal, "Aperture averaging and BER for Gaussian beam in underwater oceanic turbulence," Opt. Commun. 410, 830–835 (2018).
[34] I. Toselli and S. Gladysz, "Improving system performance by using adaptive optics and aperture averaging for laser communications in oceanic turbulence," Opt. Express 28, 17347–17361 (2020).
[35] Y. Fu, C. Huang, and Y. Du, "Effect of aperture averaging on mean bit error rate for UWOC system over moderate to strong oceanic turbulence," Opt. Commun. 451, 6–12 (2019).
[36] L. C. Andrews and R. L. Phillips, Laser Beam Propagation through Random Media (2005).
[37] M.-A. Khalighi, N. Schwartz, N. Aitamer, and S. Bourennane, "Fading reduction by aperture averaging and spatial diversity in optical wireless systems," J. Opt. Commun. Netw. 1, 580–593 (2009).
[38] Hien T. T. Pham, Minh B. Vu, Hoa T. Le, Linh D. Truong, and Ngoc T. Dang, "HAP-aided two-way relaying for FSO access networks using optical CDMA," Optical Engineering 60(9), Sept. 2021.
[39] Phuc V. Trinh, Thanh V. Pham, Ngoc T. Dang, Hung V. Nguyen, Soon xin Ng, and Anh T. Pham, "Design and Security Analysis of Quantum Key Distribution Protocol Over Free-Space Optics Using Dual-Threshold Direct-Detection Receiver," IEEE Access, vol. 06, pp. 4159–4175, 2018

APPENDIX 1: Approximation for a sum of correlated log-normal random variables

This appendix shows an approach of approximation for the summation of correlated log-normal random variables. Particularly, we can approximate $\sum_{i=1}^{k}\exp(x_k)$, where pdf of all x_k are $\Omega(x_k,-\sigma_x^2/2,\sigma_x^2)$, to single log-normal variable $Z=\exp(z)$ with pdf of z is $\Omega(z,\mu_z,\sigma_z^2)$. We can have the closed-form of mean and variance of random variable z as given by [25]

$$\mu_z=\log(k)-\frac{\sigma_z^2}{2} \text{ and } \sigma_z^2 \approx \frac{1}{k}\sigma_x^2+\frac{1}{k^2}\sum_{k\neq l}kl, \quad (34)$$

where $v_{kl}=\mathrm{cov}(x_k,x_l)$ are cross-correlation values between x_k and x_l, $k\neq l$.

BẢO MẬT LỚP VẬT LÝ CHO TRUYỀN THÔNG QUANG ĐA CHẶNG TRONG MÔI TRƯỜNG NƯỚC

Tóm tắt- Để liên lạc an toàn, nhóm nghiên cứu đề xuất một hệ thống đa truy cập phân chia theo mã (UOWC/CDMA) quang không dây dưới nước với nhiều nút hỗ trợ chuyển tiếp. Các nút chuyển tiếp sử dụng kỹ thuật phát hiện và chuyển tiếp Chip (CDF) để ngăn thủ tục giải mã nhiều người dùng. Hiệu suất hệ thống được đề xuất, về tỷ lệ lỗi bit (BER) và tính bảo mật của đường truyền, được phân tích trong nghiên cứu của chúng tôi trên các kênh fading. Trong đó, nhiễu loạn đại dương và lệch chùm tia giữa máy phát (Tx) và máy thu (Rx) có tác động tiêu cực đáng kể đến độ tin cậy của mạng UWOC. Ngoài ra, những thay đổi về chỉ số khúc xạ của nước do thay đổi áp suất, nước và nhiệt độ có thể tác động đến hoạt động của các hệ thống UWOC. Phân tích hiệu suất của liên kết UWOC dọc chịu nhiễu đa truy cập và nhiễu nền được khảo sát trong nghiên cứu này. Ngoài ra, chúng tôi khám phá đa truy cập phân chia mã quang học (CDMA), được sử dụng để hỗ trợ truyền dữ liệu đồng thời và không đồng bộ giữa các nguồn (chẳng hạn như tàu, phao, phương tiện dưới nước không người lái, thợ lặn, v.v.) và đích. Nghiên cứu này đã được thực hiện dựa trên một khung toán học chính xác để lập mô hình liên kết có tính đến các tham số kênh và Tx/Rx thực tế trong khi tính toán các tác động của nhiễu loạn đại dương và điều kiện suy hao chùm tia. Hơn nữa, nó chỉ ra rằng việc chọn các tham số Tx/Rx tốt nhất là cần thiết để đáp ứng các yêu cầu về chất lượng dịch vụ như BER và bảo mật đường truyền. Những phát hiện được cung cấp cung cấp thông tin sâu sắc về những cân nhắc thực tế khi triển khai các hệ thống UWOC/CDMA.

Từ khóa- Truyền thông không dây quang học dưới nước (UOWC), đa truy cập phân chia theo mã (CDMA), nhiễu loạn đại dương.

Nguyen Van Thang received B.E. from Posts and Telecommunications Institute of Technology (PTIT), Vietnam, in 2017. He obtained M.E. and Ph.D. degrees in Computer Science and Engineering from the University of Aizu (Japan) in 2019 and 2022, respectively. His current research interests include the aera of communication theory with a particular emphasis on modeling, design and performance analysis of hybrid FSO/RF systems, optical wireless communications, satellite communications.

Dang Tien Sy received the engineer's degree in electronics and Telecommunication from Hanoi Open University, Hanoi, Vietnam, in 2013, the master's degree in telecommunication engineering from the Posts and Telecommunications Institute of Technology (PTIT), Hanoi, Vietnam, in 2018. He is currently working for Academy of Military Science and Technology, Vietnam and joins Wireless Systems and

Applications Lab., Posts and Telecommunications Institute of Technology, Hanoi, Vietnam. His research interests on modeling, performance evaluation and secrecy of optical wireless communication and underwater wireless communication systems.

Pham Thi Thuy Hien received the B.E. Degree from Hanoi University of Transport and Communications in 1999; and the M.E. and Ph.D. degrees in Telecommunication Engineering from Posts and Telecommunications Institute of Technology (PTIT) in 2005 and 2017, respectively. She has been working at the Department of Wireless Communications of PTIT since 1999. Dr. Pham is currently a senior lecturer at PTIT. Her present research interests are in the area of design and performance evaluation of optical and wireless communication systems.